Distinction between critical current effects and intrinsic anomalies in the point-contact Andreev reflection spectra of unconventional superconductors[*]

Ge He(何格)[1,2,†,‡], Zhong-Xu Wei(魏忠旭)[1,2,†], Jérémy Brisbois[3,†], Yan-Li Jia(贾艳丽)[1,2], Yu-Long Huang(黄裕龙)[1,2],

Hua-Xue Zhou(周花雪)[1,2], Shun-Li Ni(倪顺利)[1,2], Alejandro V Silhanek[3], Lei Shan(单磊)[1,2,4],

Bei-Yi Zhu(朱北沂)[1], Jie Yuan(袁洁)[1], Xiao-Li Dong(董晓莉)[1,2,4], Fang Zhou(周放)[1,2,4],

Zhong-Xian Zhao(赵忠贤)[1,2,4], and Kui Jin(金魁)[1,2,4]

[1] Beijing National Laboratory for Condensed Matter Physics, Institute of Physics, Chinese Academy of Sciences, Beijing 100190, China

[2] School of Physical Sciences, University of Chinese Academy of Sciences, Beijing 100049, China

[3] Experimental Physics of Nanostructured Materials, Q-MAT, CESAM, Université de Liège, B-4000 Sart Tilman, Belgium

[4] Collaborative Innovation Center of Quantum Matter, Beijing 100190, China

In this work, we discuss the origin of several anomalies present in the point-contact Andreev reflection spectra of $(Li_{1-x}Fe_x)OHFeSe$, $LiTi_2O_4$, and $La_{2-x}Ce_xCuO_4$. While these features are similar to those stemming from intrinsic superconducting properties, such as Andreev reflection, electron-boson coupling, multigap superconductivity, d-wave and p-wave pairing symmetry, they cannot be accounted for by the modified Blonder–Tinkham–Klapwijk (BTK) model, but require to consider critical current effects arising from the junction geometry. Our results point to the importance of tracking the evolution of the dips and peaks in the differential conductance as a function of the bias voltage, in order to correctly deduce the properties of the superconducting state.

1. Introduction

Point-contact spectroscopy (PCS) has proved to be a simple yet powerful tool for investigating the properties of metallic and superconducting materials.[1] This technique relies on the formation of a point-contact between two metals, or a metal and a superconductor, allowing for a current I to flow through the resulting junction when a bias voltage V is applied. Typical experiments consist in measuring differential conductance $dI/dV(V)$ spectra, whose characteristic features can be associated with intrinsic material properties. On the one hand, electrons might pass from the tip to the sample by tunneling through the potential barrier at the interface. In this situation, $dI/dV(V)$ is proportional to the density of states in the sample and gives some insight into the electronic properties of the material. On the other hand, in superconducting samples, electrons with an energy smaller than the superconducting gap Δ can tunnel through the interface by pairing up with another electron to form a Cooper pair. This process,

known as Andreev reflection, leads to the reflection of a hole with opposite spin than the incident electron, in order to satisfy spin and charge conservation.[2] Point-contact spectroscopy in the Andreev reflection (PCAR) regime has been widely employed to study conventional superconductors, as $dI/dV(V)$ is strongly related to several critical properties such as Δ, pairing symmetry or electron-boson coupling, to name a few.[1,3]

In comparison to conventional superconductors, unconventional superconductors host a rich diversity of phenomena, including pseudogap,[4] d-wave/p-wave pairing symmetry[5,6] or multi-band superconductivity,[7,8] that influence the PCAR spectra. For instance, if tunneling occurs along the nodal direction, a zero bias conductance peak (ZBCP) is detected around $V = 0$. This effect, arising from the Andreev reflection between positive and negative phase in a k-dependent nodal gap,[9] was evidenced in $La_{2-x}Ce_xCuO_4$ and $YBa_2Cu_3O_{7-\delta}$.[10,11] Another example is the appearance of dips and ZBCP in the differential conductance spectra, indicating the existence of p-wave superconductivity.[12,13] This

is due to the existence of non-trivial topological edge modes. The existence of multiple energy gaps arising from multi-band superconductivity also leaves a clear imprint in the spectra, when the coupling between the gaps is weak. This was namely observed in MgB_2[14,15] and in iron-based superconductors (FeSe,[16] $(Li_{1-x}Fe_x)OHFeSe$,[17] $LaFeAsO_{0.9}F_{0.1}$,[18,19]) as evidenced by the observation of multiple coherence peaks.

Although the anomalies observed in the PCAR spectra might originate from the intrinsic properties of the unconventional superconductors under study, other less exciting phenomena related to the configuration of the junction between the tip and the sample surface should be seriously considered. Indeed, similar anomalies were widely observed both in conventional and unconventional superconductors and were attributed to diverse causes such as the superconducting proximity effect, the formation of an intergrain Josephson junction at the tip apex or heating in the point-contact, leading to a local decrease in the critical current of the superconductor.[20,21] Therefore, caution has to be exerted when interpreting the experimental data. In particular, phenomena inducing intrinsic properties of the sample and those related to the geometry might give similar features in the spectra. This could lead to erroneous conclusions on the nature of superconductivity in unconventional superconductors if the Blonder–Tinkham–Klapwijk (BTK) model,[22,23] usually employed to describe the spectra, is not amended to account for the additional effects.

In this work, we aim at clarifying the interpretation of experimental PCAR spectra, by making a clear distinction between anomalies arising from the intrinsic properties of unconventional superconductors and those coming from the junction geometry. In particular, we address the situation where the reduction of the superconducting critical current plays a crucial role in the interpretation of the data. This is the case (i) when heating occurs in the point-contact and (ii) when the tip is in series with an intergrain Josephson junction. After that we briefly review the proximity effects which will introduce similar anomalies. Under these circumstances, the results from the BTK model need to be complemented by additional contributions to account for the features in the spectra. With this in hand, we are ready to confront the theoretical description to some experimental examples of PCAR on unconventional superconductors, where it is of paramount importance to go beyond the BTK model to properly understand the superconducting properties of the sample. The experiments shed light on possible misinterpretation of the spectra, arising from the confusion between critical current effects and i) Andreev reflection, ii) multiband superconductivity, iii) p-wave superconductivity, and iv) d-wave superconductivity.

2. Modelling the critical current effects

2.1. BTK model

An ideal point-contact junction essentially consists in a metal in the non-superconducting state (N) brought in contact with a superconductor (S), separated by a thin insulating barrier (I). A simplified model, the so-called BTK model,[23] has been introduced by Blonder, Tinkham, and Klapwijk to describe PCAR in such N/I/S junctions. Assuming a unidimensional junction at zero temperature, aligned with the x axis, the repulsive insulating barrier at the interface is represented by the potential energy $U_0\delta(x)$. The transparency of the barrier is proportional to $1/(1+Z^2)$ where the parameter $Z = U_0/(\hbar v_F)$, with v_F the Fermi velocity.

Under these assumptions, the current I_{NIS} across the junction can be calculated analytically, by considering the probability of occurrence of different processes that an electron coming from the N side may undergo at the interface. In the BTK model, these include Andreev reflection (with a probability A), ordinary specular reflection (B), and transmission as an electron-like (C) or hole-like (D) quasiparticle. As a result, the current I_{NIS} can be written as

$$I_{NIS} = I_a \int_{-\infty}^{+\infty} [f(E - eV) - f(E)][1 + A(E) - B(E)]\,dE, \quad (1)$$

where V is the junction bias voltage, E is the energy, $f(E)$ is the Fermi distribution function and I_a is a constant depending on the junction constitution and geometry. The typical dependence of I_{NIS} on V is represented in Fig. 1(c) for two values of Z corresponding to extreme regimes. In all cases, for $V > \Delta/e$, the dominant conduction mechanism is the transmission of electrons through the interface as quasiparticles. For $V < \Delta/e$, the regime of conduction is strongly dependent on the value of Z. On the one hand, if Z is low, meaning that the tip is close to the sample surface, Andreev reflection dominates, as shown by the red line in Fig. 1(c). On the other hand, if the insulating layer is thick, i.e., for high Z values, the conduction is essentially dominated by tunneling, as illustrated by the blue line in Fig. 1(c). Usually, the results of PCS experiments are represented in terms of the normalized differential through its value in the normal state. Figure 1(d) shows the $dI/dV(V)$ curves corresponding to the two regimes illustrated in panel (c). The Andreev regime is characterized by an enhancement of the conductance at low V, where its value is doubled compared to the normal state. On the contrary, the hallmark of the tunneling regime is a dip at zero bias voltage.

As a final remark, note that the BTK model is valid only under the assumption that heating and proximity effects are negligible in the point-contact region. In practice, satisfying these conditions implies that the characteristic size a of the contact should be smaller than the electron mean free path l and the coherence length ξ, respectively.[8]

2.2. N/I/S junction in the intermediate regime

Up to now, we considered point-contacts with a small characteristic radius $a \ll l$, where l is the inelastic mean free path. In this situation, the electrons are in the ballistic regime and cross the point-contact without scattering, thus without dissipation. The resistance of the contact (in the normal state, $V \gg \Delta/e$) is then given by the Sharvin resistance[24]

$$R_S = \frac{4l\rho}{3\pi a^2}, \tag{2}$$

where ρ is the resistivity, proportional to l^{-1}. Therefore R_S essentially depends on the geometry of the point-contact. In the general case of a contact between two different materials, in the free-electron approximation and assuming a spherical Fermi surface for both the metal and superconductor, R_S can be written as[25]

$$R_S = \frac{2h}{e^2 a^2 k_{F,min}^2 \tau}, \tag{3}$$

where $k_{F,min} = [k_{F,m}, k_{F,s}]$ and

$$\tau = \frac{4v_{F,m}v_{F,s}}{(v_{F,m} + v_{F,s})^2}. \tag{4}$$

Parameters k_F and v_F correspond the Fermi momentum and Fermi velocity. The subscript indices m and s relate to the metal and the superconductor, respectively.

On the contrary, in the thermal regime where $l \ll a$, the resistance is mostly determined by the resistivity of the materials as given by the Maxwell resistance

$$R_M = \frac{\rho_m(T_{eff}) + \rho_s(T_{eff})}{4a}. \tag{5}$$

Since electrons are scattered in the point-contact, Joule heating occurs and the temperature T_{eff} at the center of the contact is higher than the environment temperature T and can be approximated by[26]

$$T_{eff}^2 = T^2 + \frac{V^2}{4L}, \tag{6}$$

where L is the Lorenz number. In metals, and even more so in superconductors, ρ increases as T raises. Compared to the isothermal situation, local heating will therefore result in a steeper increase of ρ as V is increased.
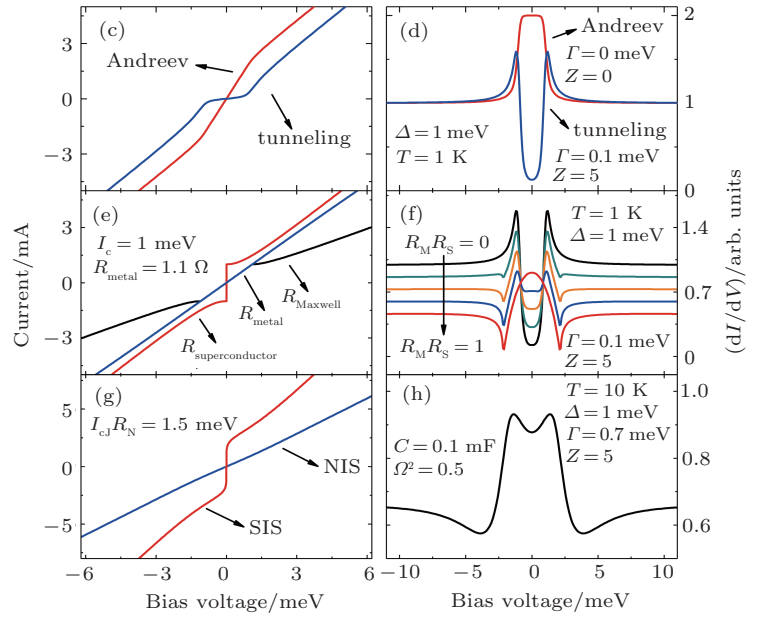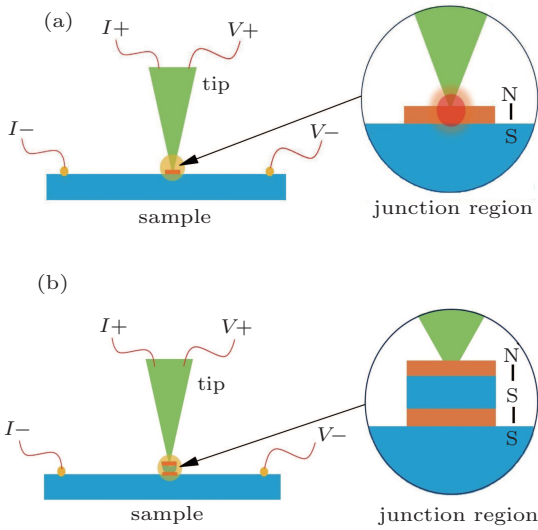
Fig. 1. (color online) Response of a point-contact when critical current effects are accounted for. (a) and (b) Schematics of the typical assembly for point-contact spectroscopy measurements, where a tip is brought into contact with the sample. The current I ($I+$ and $I-$ leads) is measured as a function of the bias voltage V ($V+$ and $V-$ leads). The enlargement of the contact region shows the simplified structure described in the theoretical model: (a) an N/I/S junction with heating and (b) an N/I/S junction in series with a Josephson junction (S/I/S). N, I, and S stand respectively for normal metal, insulator and superconductor. (c) Typical $I(V)$ dependence of the N/I/S junction calculated with the BTK model in two extremes regimes: Andreev reflection (red) and tunneling (blue). (d) Differential conductance $dI/dV(V)$ spectra corresponding to the curves in panel (c). Here Γ represents the decay of finite quasi-particle lifetime by inelastic scattering. (e) Typical $I(V)$ dependence of the Maxwell resistance R_M (black) considering the contributions of the metallic tip and the superconducting sample (red). (f) Differential conductance $dI/dV(V)$ spectra for several R_M/R_S ratios. (g) Contributions of the N/I/S (blue) and S/I/S (red) junctions to the total resistance of the junction represented in panel (b). (h) Differential conductance $dI/dV(V)$ spectra corresponding to the curves in panel (g).

In general, in the situation depicted in Fig. 1(a), the point-contact lies in an intermediate regime where the total resistance R is made of the combined contributions of R_S and R_M[27]

$$R = R_S + \Gamma\left(\frac{l}{a}\right)R_M, \tag{7}$$

where the function $\Gamma(l/a)$ is on the order of 1 and varies slowly with l/a. Since $R_S \sim a^{-2}$, while $R_M \sim a^{-1}$, the resis-

tance of small contacts is dominated by R_S, while R_M becomes preponderant for large contacts.

The features of R_S have been described previously by the BTK model. The $I(V)$ characteristics of R_M can be plotted using Eq. (5) as shown in Fig. 1(e). The red curve gives an example of a typical $I(V)$ curve for a superconductor, while the metal is represented in blue. If a current is applied to measure the $I(V)$ curve of the junction, the total voltage of the junction from Maxwell resistance is the sum of V_{metal} and $V_{superconductor}$. At a current higher than the critical current (I_c) of the superconductor, the superconductor turns into a normal metal. Thus, the $I(V)$ curve obeys the Ohm's law. However, when the current is close to I_c, the resistance of the superconductor decreases rapidly and the total voltage decreases, leading to the observation of a prominent nonlinear feature. Until a current lower than I_c, the $I(V)$ characteristics are determined by the metal. Most of time, due to the heating effect, the $I(V)$ curve might deviate from the linear behavior in this regime, depending on the effective temperature governed by Eq. (6). Tuning the value of R_M/R_S, we obtain a normalized $dI/dV(V)$ spectra as represented in Fig. 1(f). Due to the existence of I_c in the superconductor, two dips can be observed in the spectra in the intermediate regime. With the decrease of R_M/R_S, the magnitude of the dip decreases gradually.

2.3. Critical current effects in N/I/S and S/I/S (S/N/S) junctions in series

In polycrystalline superconductors, where the intergrain weak-coupling effect plays an important role, the BTK model does no longer provide a satisfying description of the junction. Indeed, in this situation, the junction between the tip and the sample surface can in general be represented by the point-contact (N/I/S) described previously, associated in series with a Josephson junction (S/I/S), accounting for the connection between the tip and the superconducting grains. This situation is depicted in Fig. 1(b).

The total voltage V across the junction is then the sum of two contributions: the point-contact voltage V_{NIS}, described by the BTK model, and the Josephson junction voltage V_{SIS}. In the presence of thermal noise and with the assumption that the associated capacitance C is small, the contribution of V_{SIS} can be calculated by the resistively shunted junction (RSJ) model,[20,28] and is written as

$$V_{SIS} = \frac{2R_N I_{cJ}}{\gamma} \frac{\exp(\pi\gamma I/I_{cJ}) - 1}{\exp(\pi\gamma I/I_{cJ})} T_1^{-1} \left(1 + \Omega^2 \frac{T_2}{T_1}\right), \quad (8)$$

$$T_1 = \int_0^{2\pi} d\phi\, I_0\left(\gamma\sin\left(\frac{\phi}{2}\right)\right) \exp\left(-\frac{\gamma\phi I}{2I_{cJ}}\right), \quad (9)$$

$$T_2 = \int_0^{2\pi} d\phi\, \sin\left(\frac{\phi}{2}\right) I_1\left(\gamma\sin\left(\frac{\phi}{2}\right)\right) \exp\left(-\frac{\gamma\phi I}{2I_{cJ}}\right), \quad (10)$$

where I_0 and I_1 are the modified Bessel functions, R_N is the normal state resistance, I_{cJ} is the maximum Josephson current, $\gamma = hI_{cJ}/ek_B T_n$, in which T_n is the effective noise temperature, and $\Omega = (2eI_{cJ}C/\hbar)^{1/2} T_n$.

The $I(V)$ curve corresponding to the typical response of a Josephson junction is shown in red in Fig. 1(g). In general, at $I < I_{cJ}$, only Cooper pairs are able to pass through the junction, and V remains small. However, at $I > I_{cJ}$, the Cooper channel gradually vanishes, whereas the Josephson junction $I(V)$ turns to the quasiparticle branch with a certain normal resistance.

The features of the spectra resulting from the association of the NIS junction and SIS junction depend strongly on their normal-state resistances R_{NIS} and R_{SIS}, respectively. We can calculate the $I(V)$ characteristic and the differential conductance by using the following relations: $V(I) = V_{NIS} + V_{SIS}$, $dI/dV(V) = (dV/dI_{NIS}(V) + dV/dI_{SIS}(V))^{-1}$. When current is lower than I_{cJ}, V_{SIS} is close to 0, and V_{NIS} dominates the total voltage. However, with the increase of current, a remark enhancement of V_{SIS} happens at I_{cJ}, which leads to two dips in the $dI/dV(V)$ curve as seen in Fig. 1(h).

In some point-contacts, the tip is not sharp enough, and Andreev reflection effect becomes weaker than a fine junction. In this case, SIS junction dominates the spectrum, and a ZBCP can be observed, which is higher than 2[20,29] (the maximum value expected from the conventional Andreev reflection). It is known that ZBCP is not expected for an ideal RSJ model except for a point of divergence at zero point. However, when a small normal R_{NIS} connect in series with R_{SIS}, at $V < 2\Delta/e$, $I(V)$ curve has a large slope but not a vertical line, where the ZBCP can be observed. It is expected to observe two coherence peaks and ZBCP at the same time in an appropriate situation.

Finally, if the insulating layer in the SIS is substituted by a normal metal, i.e., SNS, multiple Andreev reflection may happen at the interface between the superconductor and the metal, which can also induce an enhanced ZBCP higher than 2.

2.4. Proximity effects

Proximity effects occurring at the interface between a metal and a superconductor might give rise to additional features in the conductance spectra.[30] Indeed, due to the diffusion of Cooper pairs from the superconductor to the metal, a weak superconducting layer is formed at the superconductor/metal interface, with a superconducting gap smaller than the bulk value. Therefore, Andreev reflection in the proximity effect layer occurs for voltages lower than the bulk value. However, the bias voltage still needs to be large enough to overcome the bulk gap, so a dip in the conductance spectrum

appears between those values. The proximity effect can be accounted for by introducing two gap values in the model, giving rise to sharp dips between the voltages corresponding to the gap energies. This effect is more prominent in the case of a clean contact with a low Z.

3. Results and discussion

3.1. Experimental details

The point-contact junctions between the samples and the probe are established using home-made Pt/Ir tips or a small drop of Ag paste. The assembly is installed in a Quantum Design PPMS system to achieve temperatures as low as 1.8 K, and high magnetic fields, up to 15 T. Sample stage motion is allowed on the x-axis and z-axis, in the range of 3 mm and 2.5 mm respectively. The differential conductance dI/dV, is measured as a function of the bias voltage V by a standard lock-in technique. The methods of growing the $La_{2-x}Ce_xCuO_4$[31] films, $LiTi_2O_4$[32] films, $(Li_{1-x}Fe_x)OHFeSe$ crystals,[33] and films[34] can be found elsewhere.

3.2. Distinction between critical current effects and Andreev reflection

The experimental PCAR spectra obtained on a point-contact between an $(Li_{1-x}Fe_x)OHFeSe$ sample and a PtIr tip are shown in Fig. 2(a), for temperatures between 5 K and 40 K. The inset represents corresponding $I(V)$ curve at $T = 5$ K which is obviously nonlinear. The critical temperature of the sample is $T_c = 38$ K. A marked peak with an amplitude over 4 is present in the signal at low temperature. Its strength decreases as T increases and it vanishes around $T \sim T_c$. At first sight, this feature seems related to the Andreev reflection observed for superconducting samples. However, a careful comparison with the BTK theory, represented in Fig. 2(b) for temperatures between $0.5T_c$ and T_c, shows that Andreev reflection alone cannot account for the observed experimental spectra, as the shape and amplitude of the peak is significantly different. The fitting of the experimental spectrum at $T = 20$ K, represented in the inset of Fig. 2(b), clearly illustrates this point. As a consequence, if the BTK model is used to fit this data, incorrect information will be obtained on the superconducting properties, such as the superconducting gap Δ.
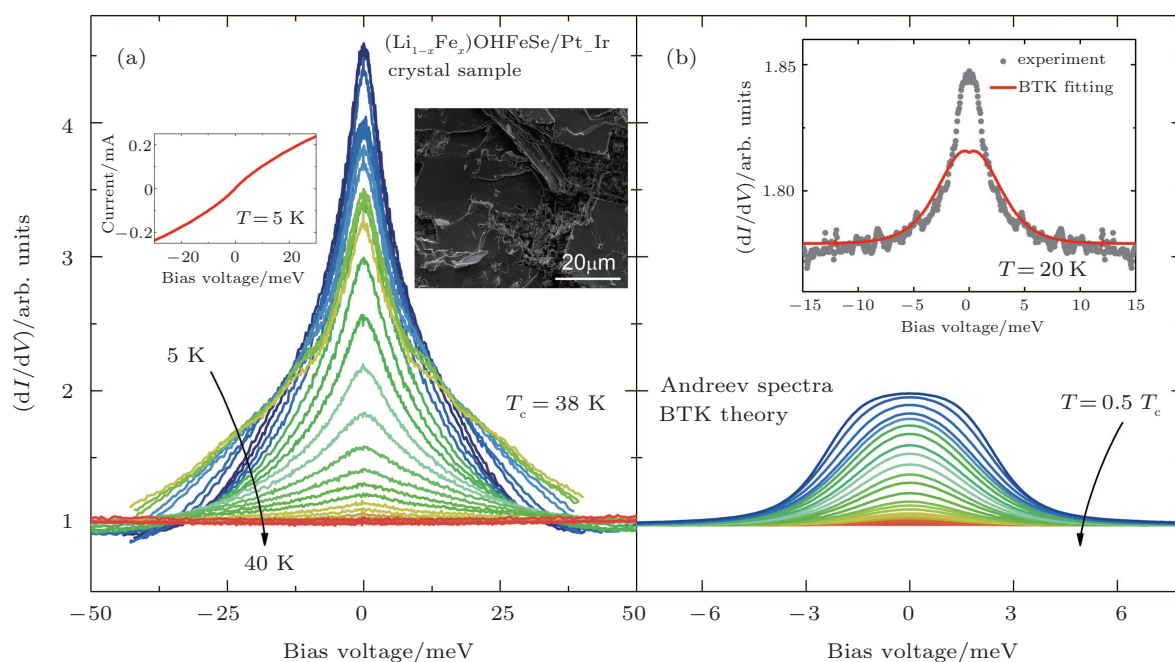
Fig. 2. (color online) Distinction between critical current effects and Andreev reflection. (a) PCAR spectra on an $(Li_{1-x}Fe_x)OHFeSe$ sample with $T_c = 38$ K for temperatures between 5 K and 40 K. The inset shows the corresponding $I(V)$ dependence at $T = 5$ K and the picture of surface taken by the scanning electron microscope. (b) Andreev reflection spectra obtained by calculations within the framework of the BTK model for temperatures between $0.5T_c$ and T_c. The inset shows the clear discrepancy between the experimental curve at $T = 20$ K (dots) and the result of fitting with the BTK model (red line).

The differences between the experimental spectra and the BTK model can be attributed to critical current effects, arising from the formation of an S/I/S(S/N/S) junction at the apex of the tip or the thermal effect. Indeed, as explained previously, the response of such a junction might lead to a large peak at zero bias, with amplitude significantly larger than 2. In view

of the picture taken by scanning electron microscope showing easily broken surface [See the inset in Fig. 2(a)], we prefer the case of weak-links between superconducting grains. The peak amplitude observed in the data can therefore be decomposed in two contributions coming from the Andreev reflection, with an amplitude close to 2, and the Josephson junction accounting

for the rest. Moreover, the peak is sharper than for Andreev reflection, in agreement with the N/I/S + S/I/S(S/N/S) model we exposed above.

These spectra are usually observed in iron-based superconductors,[3] such as the sample we studied here, as their surface is often fragile. As a consequence, in the process of forming a point-contact between the tip and the sample, the surface frequently suffers degradation. The resulting debris or defects lead to the formation of an S/I/S(S/N/S) junction between the tip apex and the sample. Another possible explanation for the formation of these junctions involves the bad crystallinity of some samples, such as polycrystalline systems, where the intergrain coupling plays a significant role. A more compelling evidence would require nanoscopic imagin of the tip-sample interface which is not straighforward even with the technology available today.

3.3. Distinction between critical current effects and multiband or p-wave superconductivity

Various unconventional superconductors were found to exhibit a multiband behavior.[14,35–37] For instance, in iron-based superconductors, Angle-Resolved Photoemission Spectroscopy (ARPES) measurements widely show a signature of multiband superconductivity, with a hole pocket in the Γ points and an electron pocket in the M point.[36,38] In these systems, PCAR spectroscopy is a tool of choice to extract information on the band coupling. In many compounds, such as FeSe[16] and $(Li_{1-x}Fe_x)OHFeSe$,[17] the spectra point to the existence of two superconducting gaps. However, caution has to be exerted when interpreting $dI/dV(V)$ spectra, as the dips characteristic of multiband superconductivity look very similar to those induced by critical current effects.
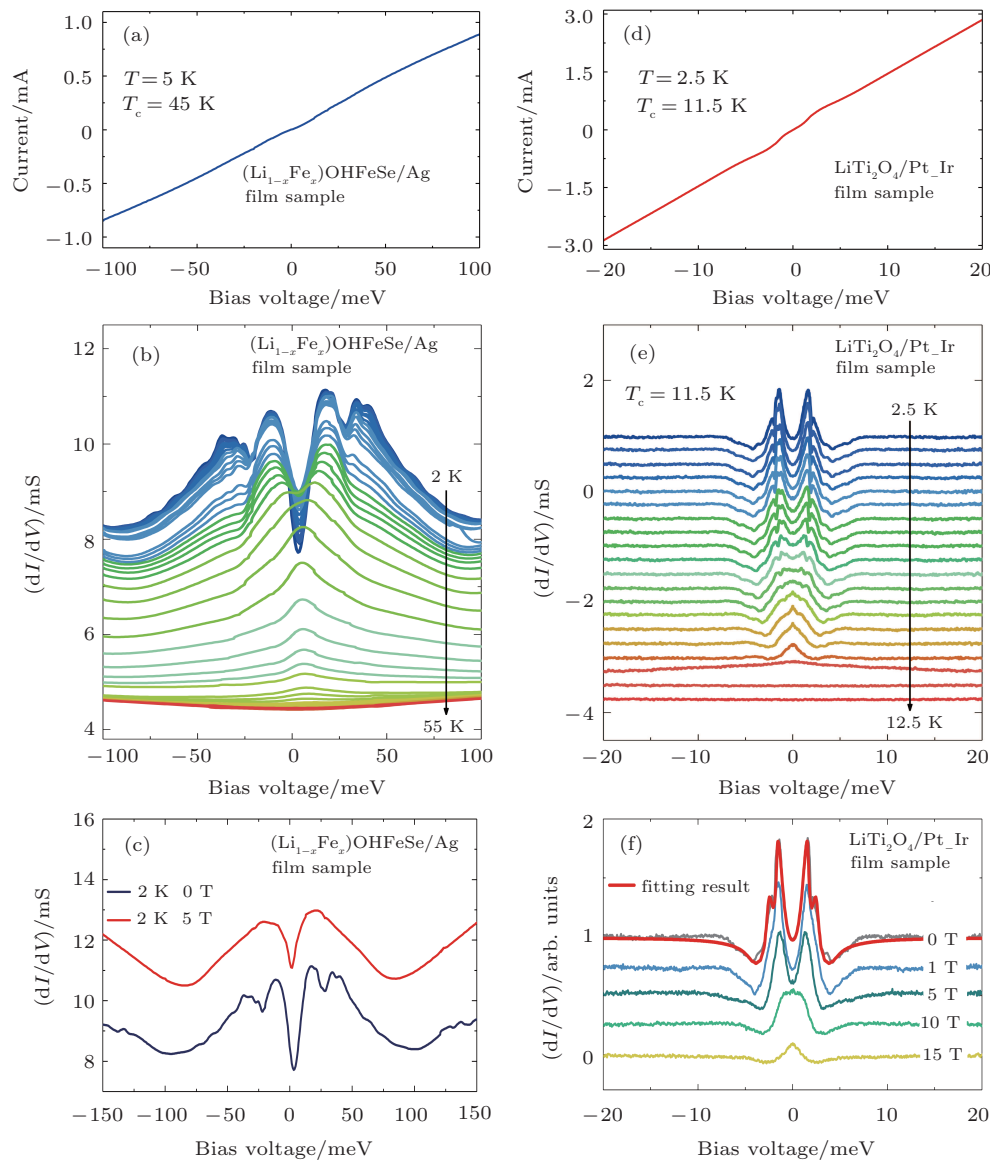
Fig. 3. (color online) Distinction between critical current effects and multiband or p-wave superconductivity. (a) The $I(V)$ curve of $(Li_{1-x}Fe_x)OHFeSe$ film at $T = 2$ K with a critical temperature $T_c = 45$ K. (b) $dI/dV(V)$ spectra of $(Li_{1-x}Fe_x)OHFeSe$ film, for T between 2 K and 55 K. (c) $dI/dV(V)$ spectra of $(Li_{1-x}Fe_x)OHFeSe$ at 2 K for a magnetic field $\mu_0H = 0$ T (blue line) and $\mu_0H = 5$ T (red line). (d) The $I(V)$ dependence of $LiTi_2O_4$ film at $T = 2.5$ K with a critical temperature $T_c = 11.5$ K. (e) $dI/dV(V)$ spectra of $LiTi_2O_4$ film, for T between 2.5 K and 12.5 K. (f) $dI/dV(V)$ spectra of $LiTi_2O_4$ for magnetic fields between 0 T (blue line) and 15 T (red line) at 2.5 K.

Figure 3(b) shows the experimental $dI/dV(V)$ spectra for an $(Li_{1-x}Fe_x)OHFeSe$ film with a critical temperature $T_c = 45$ K. Measurements are taken at temperatures ranging from 2 K to 55 K. At first sight, the dip structure might suggest the existence of multiband superconductivity. However, a more careful look shows that this explanation is incorrect and that the features in the spectra are actually explained by critical current effects. First, the energy scale associated with the dips is as high as 40 meV, while the features disappear at $T \sim 26$ K. These values give a coupling constant $2\Delta/k_BT_c \sim 33$, much larger than the BCS value of 3.53, and are thus incompatible with the hypothesis of a BCS superconducting gap. This is further supported by the magnetic field dependence of the spectra, illustrated in Fig. 3(c) at 2 K for $\mu_0H = 0$ T (blue line) and $\mu_0H = 5$ T (red line), showing that the dips disappear at fields below 5 T. However, it is well known that in $(Li_{1-x}Fe_x)OHFeSe$ samples, the upper critical field H_{c2} is typically larger than 100 T.[39] The suppression of the dips at $T < T_c$ and $H < H_{c2}$ is due to the fact that the tip locally depletes superconductivity, possibly forming S/I/S junctions in the process. On the other hand, the $I(V)$ curve at $T = 5$ K in Fig. 3(a) shows many bends, which also indicate the $dI/dV(V)$ spectra contain some intrinsic information.

For p-wave superconductors, PCAR spectra show double dips and ZBCP, resulting from the existence of non-trivial edge modes in unconventional topological superconductors.[13] These features have been observed in $Cu_xBi_2Se_3$,[12] Cd_3As_2,[40] and TaAs.[41] We performed PCAR measurements on a $LiTi_2O_4$ film ($T_c = 11$ K). Fig. 3(d) shows the $I(V)$ curve at $T = 2.5$ K. The characteristics of the curve are similar to those of the $(Li_{1-x}Fe_x)OHFeSe$ film. The resulting $dI/dV(V)$ spectra are shown in Fig. 3(e) for temperatures between 2.5 K and 12.5 K. Double dips and peaks features are present at low temperatures, while a single ZBCP is visible at higher temperatures. Figure 3(f) illustrates the magnetic field dependence of the signal. Increasing the field leads to a gradual change of the features to a single ZBCP with two shallow dips.

However, the experimental features cannot be attributed to p-wave superconductivity, since $LiTi_2O_4$ is a normal metal without topological features in band structure.[42,43] This is also backed up by other experimental techniques, such as point contact measurements[44] and specific heat measurements,[45] that clearly point to the existence of s-wave superconductivity. The observed features can however be explained by critical current effects. This is further supported by the fact that in both samples sets, increasing T or H leads to the disappearance of the small irregularities in the spectra, attributed to weak-links between superconducting grains. As for the split peaks observed in spectra, it can be generated by several mechanisms: proximity effect, two superconducting gaps,

and weak-links between superconducting grains. The case of two superconducting gaps can be ruled out through the analysis above. We firstly try to fit this anomaly by proximity effect. However, the fitting result is not ideal even trying much different values of fitting parameters. On the contrary, the features like double dips and two split peaks can be well fitted by the model of an N/I/S junction in series with two S/I/S junctions at the same time, as shown in Fig. 3(f).

Strong electron–boson coupling might also be invoked to explain the humps/dips features in the tunneling spectra,[46–48] by establishing a correspondence with the electron–boson spectra function $\alpha^2F(w)$, where w is the boson energy. These features are observed in various cuprate[48] and iron-based superconductors,[46,47] as well as in $LiTi_2O_4$.[49] In this situation, the spectra provides fingerprint information to resolve the nature of superconductivity. The energy scale can be exploited to discriminate between the possible origin of the features in the spectra. Indeed, while the energy scale is strongly dependent on the point-contact geometry in the case of a spectrum dominated by critical current effects, it is pretty much unaffected by the position for electron-boson coupling.

3.4. Distinction between critical current effects and d-wave superconductivity

In cuprate superconductors, the $d_{x^2-y^2}$-wave pairing symmetry mechanism is widely accepted, as it has been established by phase-sensitive techniques,[5] Raman[50] or tunneling spectroscopy,[10,11] to name a few. In a superconductor with $d_{x^2-y^2}$-wave symmetry, the gap function is typically given by

$$\Delta\left(\theta_{\pm}\right) = \Delta_0 \cos\left(2\theta \mp 2\alpha\right), \tag{11}$$

where α is the angle between the a axis of the sample and the axis of the N/I/S junction.

A characteristic feature of superconductors with d-wave symmetry is the ZBCP observed in the PCAR spectra, stemming from Andreev reflection occurring between positive and negative phases in a k-dependent node gap.[9,51] However, the particular shape of the spectra is strongly dependent on α, and dips and peaks might appear as the angle is changed. In contrast to the Andreev reflection spectra for an s-wave superconductor, the zero bias conductance might be larger than 2, thus making it difficult to distinguish from critical current effects. Figure 4 summarizes the PCAR results on an $La_{0.9}Ce_{0.1}CuO_4$ film with a critical temperature $T_c = 25$ K. The $dI/dV(V)$ spectrum at $T = 1.8$ K, represented in Fig. 4(a), shows a clear ZBCP. As the temperature is increased up to 25 K (see the gray lines in panels (c) and (d)), the shape of the spectra evolves to a single peak at zero bias. However, while fitting of the spectra with the d-wave BTK theory works well at low temperatures,

as represented by the red line in Fig. 4(c), it is clearly inadequate at higher temperatures, as illustrated in Fig. 4(d). Moreover, as shown in Fig. 4(b), the normalized intensity of the ZBCP, dI/d$V(0)$, increases slowly below 20 K and is abruptly enhanced above 20 K, while finally disappearing close to T_c. This behavior is in contradiction with the expectations for a ZBCP induced by d-wave superconductivity, that should decrease monotonously as the temperature raises.
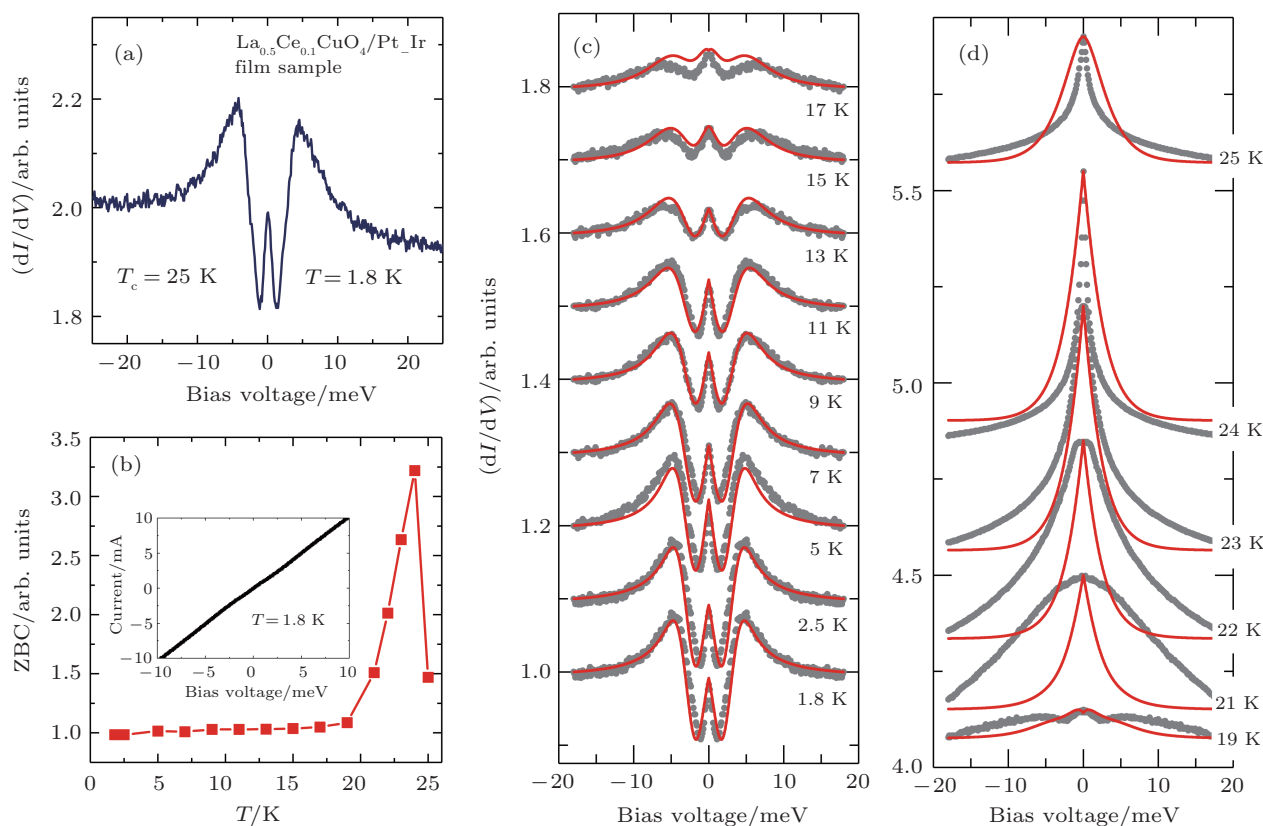
Fig. 4. (color online) Distinction between critical current effects and zero bias conductance peak. (a) dI/d$V(V)$ spectra for an La$_{0.9}$Ce$_{0.1}$CuO$_4$ film with a critical temperature $T_c = 25$ K at $T = 1.8$ K. (b) Evolution of dI/d$V(0)$ (zero bias conductance) with the temperature, obtained from the dI/d$V(V)$ spectra represented in panels (c) and (d). The experimental data is shown in gray, while fitting with the BTK model is represented by the red line. The inset in panel (b) shows the corresponding $I(V)$ curve at $T = 1.8$ K.

The ZBCP observed in LCCO can be satisfyingly explained by invoking critical current effects. The sharp increase of the dI/d$V(0)$ value observed when the temperature raises, as opposed to the situation in Fig. 2(a) for instance, might come from the influence of the thermal effects, impacting significantly the conduction regime in the junction. When temperature goes to T_c, the superconductivity of the sample will be suppressed, which result in weakening of the critical current effect. In general, the increase or decrease of ZBCP depends on the competition between both two effects. For higher temperature, we can only obtain a normal state spectra without ZBCP induced by critical current effects because the sample is in normal state.

4. Conclusion

Point-contact spectroscopy in the Andreev reflection regime constitutes a tool of choice to study unconventional superconductors. Indeed, some of the features observed in the differential conductance dI/d$V(V)$ spectra can be attributed to intrinsic properties of the superconducting material, such as Andreev reflection, electron–boson coupling, multigap superconductivity, d-wave and p-wave pairing symmetry. Unfortunately, the resulting anomalies are very similar to those stemming from the critical current effects related to the junction geometry. We reviewed the models accounting for the critical current effects where additional contributions to the resistance of the junction, not considered in the modified BTK model, are included. As a consequence, the differential conductance spectra present a wide variety of features, ranging from zero bias conductance peak to dips, depending on the relative importance of the contributions to the total junction resistance. We provide some experimental evidence of situations where it is crucial to take the critical current effects into account in order to properly describe the superconducting properties.

References

[1] Deutscher G 2005 *Rev. Mod. Phys.* **77** 109
[2] Andreev A F 1964 *Sov. Phys. JETP* **19** 1228
[3] Daghero D, Tortello M , Ummarino G A and Gonnelli R S 2011 *Rep. Prog. Phys.* **74** 124509
[4] Ding H, Yokoya T, Campuzano J C, Takahashi T, Randeria M, Norman M R, Mochiku T, Kadowaki K and Giapintzakis J 1996 *Nature* **382** 51

[5] Tsuei C C and Kirtley J R 2000 *Phys. Rev. Lett.* **85** 182

[6] Ott H R, Rudigier H, Rice T M, Ueda K, Fisk Z and Smith J L 1984 *Phys. Rev. Lett.* **52** 1915

[7] Paglione J and Greene R L 2010 *Nature Phys.* **6** 645

[8] Daghero D and Gonnelli R S 2010 *Supercond. Sci. Tech.* **23** 043001

[9] VanHarlingen D 1995 *Rev. Mod. Phys.* **67** 515

[10] Chesca B, Ehrhardt K, Möβle M, Straub R, Koelle D, Kleiner R and Tsukada A 2003 *Phys. Rev. Lett.* **90** 057004

[11] Sharoni A, Koren G and Millo O 2001 *Euro. Lett.* **54** 675

[12] Sasaki S, Kriener M, Segawa K, Yada K, Tanaka Y, Sato M and Ando Y 2011 *Phys. Rev. Lett.* **107** 217001

[13] Takami S, Yada K, Yamakage A, Sato M and Tanaka Y 2014 *J. Phys. Soc. Jpn.* **83** 064705

[14] Gonnelli R S, Daghero D, Ummarino G A, Stepanov V A, Jun J, Kazakov S M and Karpinski J 2002 *Phys. Rev. Lett.* **89** 247004

[15] Hol'anová Z, Szabó P, Samuely P, Wilke R H T, Bud'ko S L and Canfield P C 2004 *Phys. Rev. B* **70** 064520

[16] Wang Q Y, Li Z, Zhang W H, Zhang Z C, Zhang J S, Li W, Ding H, Ou Y B, Deng P, Chang K, Wen J, Song C L, He K, Jia J F, Ji S H, Wang Y Y, Wang L L, Chen X, Ma X C and Xue Q K 2012 *Chin. Phys. Lett.* **29** 037402

[17] Du Z Y, Yang X, Lin H, Fang D L, Du G, Xing J, Yang H, Zhu X Y and Wen H H 2016 *Nature Communi.* **7** 10565

[18] Gonnelli R S, Tortello M, Daghero D, Ummarino G A, Stepanov V A and Kim J S 2009 *Cent. Eur. J. Phys.* **7** 251-256

[19] Gonnelli R S, Daghero D, Tortello M, Ummarino G A, Stepanov V A, Kim J S and Kremer R K 2009 *Phys. Rev. B* **79** 184526

[20] Shan L, Tao H J, Gao H, Li Z Z, Ren Z A, Che G C and Wen H H 2003 *Phys. Rev. B* **68** 144510

[21] Sheet G, Mukhopadhyay S and Raychaudhuri P 2004 *Phys. Rev. B* **69** 134507

[22] Blonder G, Tinkham M and Klapwijk T 1982 *Phys. Rev. B* **25** 4515

[23] Blonder G and Tinkham M 1983 *Phys. Rev. B* **27** 112

[24] Sharvin Y V 1965 *Sov. Phys. JETP* **21** 655

[25] Baranger H U, MacDonald A H and Leavens C R 1985 *Phys. Rev. B* **31** 6197

[26] Duif A M, Jansen A G M and Wyder P 1989 *J. Phys. Cond. Matt.* **1** 3157-3189

[27] Wexler G 1996 *Proc. Phys. Soc. London* **89** 927

[28] Lee P A 1971 *J. Appl. Phys.* **42** 325

[29] Mao Z Q, Rosario M M, Nelson K D, Wu K, Deac I G, Schiffer P, Liu Y, He T, Regan K A and Cava R J 2003 *Phys. Rev. B* **67** 094502

[30] Strijkers G J, Ji Y, Yang F Y, Chien C L and Byers J M 2001 *Phys. Rev. B* **63** 104510

[31] Jin K, Butch N P, Kirshenbaum K, Paglione J and Greene R L 2011 *Nature* **476** 73

[32] Jia Y L, He G and Hu W and Yang H and Yang Z Z and Yu H S and Zhang Q H and Shi J A and Lin Z F and Yuan J and Zhu B Y and Gu L and Li H and Jin K 2017 arXiv: 1706.07618

[33] Dong X L, Jin K, Yuan D N, Zhou H X, Yuan J, Huang Y L, Hua W, Sun J L, Zheng P and Hu W 2015 *Phys. Rev. B* **92** 064515

[34] Huang Y L, Feng Z P, Ni S L, Li J, Hu W, Liu S B, Mao Y Y, Zhou H X, Zhou F, Jin K, Wang H B, Yuan J, Dong X L and Zhao Z X 2017 *Chin. Phys. Lett.* **34** 077404

[35] Armitage N P, Ronning F, Lu D H, Kim C, Damascelli A, Shen K M, Feng D L, Eisaki H, Shen Z X, Onose Y, Taguchi Y and Tokura Y 2002 *Phys. Rev. Lett.* **88** 257001

[36] Zhao L, Liang A, Yuan D, Hu Y, Liu D, Huang J, He S, Shen B, Xu Y, Liu X, Yu L, Liu G, Zhou H, Huang Y, Dong X, Zhou F, Liu K, Lu Z, Zhao Z, Chen C, Xu Z and Zhou X J 2016 *Nat. Commun.* **7** 10608

[37] Putzke C, Coldea A I, Guillamón I, Vignolles D, McCollam A, Leboeuf D, Watson M D, Mazin I I, Kasahara S, Terashima T, Shibauchi T, Matsuda Y and Carrington A 2012 *Phys. Rev. Lett.* **108** 047002

[38] Shimojima T, Suzuki Y, Sonobe T, Nakamura A, Sakano M, Omachi J, Yoshioka K, Kuwata-Gonokami M, Ono K, Kumigashira H, Böhmer A E, Hardy F, Wolf T, Meingast C, Löhneysen H V, Ikeda H and Ishizaka K 2014 *Phys. Rev. B* **90** 121111

[39] Dong X L, Jin K, Yuan D N, Zhou H X, Yuan J, Huang Y L, Hua W, Sun J L, Zheng P, Hu W, Mao Y Y, Ma M W, Zhang G M, Zhou F and Zhao Z X 2015 *Phys. Rev. B* **92** 064515

[40] Wang H, Wang H, Liu H, Lu H, Yang W, Jia S, Liu X J, Xie X C, Wei J and Wang J 2016 *Nature Mater.* **15** 38

[41] Wang H, Wang H C, Chen Y Q, Luo J W, Yuan Z J, Liu J, Wang Y, Jia S, Liu X J, Wei J and Wang J 2017 *Sci. Bull.* **62** 425

[42] Satpathy S and Martin R 1987 *Phys. Rev. B* **36** 7269

[43] Massidda S, Yu J and Freeman A 1988 *Phys. Rev. B* **38** 11352

[44] Jin K, He G, Zhang X, Maruyama S, Yasui S, Suchoski R, Shin J, Jiang Y, Yu H S, Yuan J, Shan L, Kusmartsev F V, Greene R L and Takeuchi I 2015 *Nature Communi.* **6** 7183

[45] Sun C, Lin J Y, Mollah S, Ho P, Yang H, Hsu F, Liao Y and Wu M 2004 *Phys. Rev. B* **70** 054519

[46] Shan L, Gong J, Wang Y L, Shen B, Hou X Y, Ren C, Li C H, Yang H, Wen H H, Li S L and Dai P C 2012 *Phys. Rev. Lett.* **108** 227002

[47] Chi S, Grothe S, Liang R, Dosanjh P, Hardy W N, Burke S A, Bonn D A and Pennec Y 2012 *Phys. Rev. Lett.* **109** 087002

[48] Niestemski F C, Kunwar S, Zhou S, Li S, Ding H, Wang Z, Dai P and Madhavan V 2007 *Nature* **450** 7172

[49] He G, Jia Y L, Hou X Y, Wei Z X, Xie H D, Yang Z Z, Shi J A, Yuan J, Shan L, Zhu B Y, Li H, Gu L, Liu K, Xiang T and Jin K 2017 *Phys. Rev. B* **95** 054510

[50] Blumberg G, Koitzsch A, Gozar A, Dennis B, Kendziora C, Fournier P and Greene R 2002 *Phys. Rev. Lett.* **88** 107002

[51] Tanaka Y and Kashiwaya S 1995 *Phys. Rev. Lett.* **74** 3451